第 34 卷第 11 期
2018 年 11 月

无 机 化 学 学 报
CHINESE JOURNAL OF INORGANIC CHEMISTRY

Vol.34 No.11
2115-2126

La 掺杂在 BiOBr 光催化剂氧化和还原性能调控中的不同作用

樊启哲[1] 廖春发*,[1] 李之锋[2] 张志文[1] 陈 鑫[1] 余长林*,[1]

([1]江西理工大学冶金与化学工程学院,赣州 341000)

([2]江西理工大学材料科学与工程学院,赣州 341000)

摘要:同时使用有机溴源十六烷基三甲基溴化铵(CTAB)和无机溴源 NaBr,通过溶剂热法合成了具有层状类囊体结构的 La 掺杂 BiOBr 光催化剂。通过第一性原理(DFT)计算了 La 掺杂对 BiOBr 能带结构的影响。采用 X 射线衍射、扫描电子显微镜、透射电子显微镜、X 射线光电子能谱及荧光光谱对催化剂进行了表征。在可见光照射下,以光催化降解酸性橙Ⅱ和氨氮废水测试了 La-BiOBr 的氧化性能;以亚甲基蓝为还原指示剂,测试了 La-BiOBr 的还原性能。研究表明,La 的掺杂可以促进晶粒的堆积。而且 BiOBr 的氧化性能和还原性能分别被促进和抑制,即 La 的掺杂促进了 BiOBr 光催化剂的氧化性能,抑制了其还原性能。

关键词:光催化;光氧化;卤氧化铋;镧;掺杂

中图分类号:O643.3;TB34 **文献标识码**:A **文章编号**:1001-4861(2018)11-2115-12

DOI:10.11862/CJIC.2018.255

Distinct Role of La Doping in Regulating the Photo-Oxidation and Reduction of BiOBr Nanosheet

FAN Qi-Zhe[1] LIAO Chun-Fa*,[1] LI Zhi-Feng[2] ZHANG Zhi-Wen[1] CHEN Xin[1] YU Chang-Lin*,[1]

([1]*School of Metallurgy and Chemical Engineering, Jiangxi University of Science and Technology, Ganzhou, Jiangxi* 341000, *China*)

([2]*School of Materials Science and Engineering, Jiangxi University of Science and Technology, Ganzhou, Jiangxi* 341000, *China*)

Abstract: Both organic cetyltrimethyl ammonium bromide (CTAB) and inorganic NaBr are served as the bromine source, the thylakoid-like La doped BiOBr photocatalysts were synthesized via a hydrothermal process. The obtained samples were first characterized by X-ray diffraction (XRD), N_2 physical adsorption, scanning electron microscopy (SEM), transmission electron microscopy (TEM), UV-visible spectroscopy, X-ray photoelectron spectroscopy (XPS) and photoluminescence (PL) spectroscopy. Then, the effects of photo-oxidation and reduction properties of BiOBr with La doping were investigated by DFT calculation. The photo-oxidation and reduction activity of the pure and La doped BiOBr samples were evaluated by photo-catalytic degradation of acid orange Ⅱ, ammonia nitrogen and methylene blue reduction under visible light irradiation. The results showed that it could inhibit growth of BiOBr crystals and promote the stacking crystals when La doped. More importantly, the oxidation performances of BiOBr were promoted, where the reduction performances were inhibited in large part by La doping.

Keywords: photocatalysis; photo-oxidation; bismuth halide oxides; lanthanum; doping

收稿日期:2018-07-26。收修改稿日期:2018-09-04。

国家自然科学基金(No.21567008),江西省 5511 科技创新人才项目(No.20165BCB18014),江西省主要学科学术和技术带头人资助计划(No.20172BCB22018),江西省教育厅科学技术研究项目(No.GJJ150630),江西省研究生创新专项资金项目(No.YC2016-B076),赣州市工业技术创新项目(2015),江西理工大学优秀博士学位论文培育计划项目(No.YB2016006),江西理工大学科研基金(No.NSFJ2015-G08)和江西理工大学大学生创新训练项目(No.DC2017-014)。

*通信联系人。E-mail:yuchanglinjx@163.com,liaochfa@163.com

0 Introduction

It is well known that the photo catalytic efficiency is determined by the oxidation and reduction ability of photo catalyst. Therefore, there are mainly two aspects applications for photocatalyst. One is the oxidation property, which is used for decomposition or mineralization of the organic pollutants to CO_2 and H_2O[1-8]. Another is the photoreduction which was applied to reduce CO_2 into CH_3OH (CO, CH_4)[9-11], H_2O into H_2[12-15], N_2 to NH_3[16]. It is known that the photo-oxidation and reduction property of photocatalyst was closely related to its band and energy structure. Therefore, if the location of the valence band and the conduction band can be precisely regulated, we could obtain the photocatalyst with superior strong oxidation or reduction performance.

Recently, the performances of bismuth oxyhalide (BiOX) in photocatalytic degradation of organic compounds have aroused much attention[17-23]. The unique layered structure and anisotropic property of bismuth oxyhalide (BiOX) semiconductor bring about the big advantage to regulate their band and energy structures. It is interesting to note that rare earth element lanthanum can effectively influence crystal growth[24]. Moreover, the built-in electric field and catalytic active center in BiOX crystals could be effectively regulated by doped lanthanum cation due to its abundant charges with $[Xe]5d^16s^2$ electronic configuration. Although there are some reports about rare earth doped BiOX (X=Cl, Br, I), *e.g.* Eu^{3+}-doped BiOX[25-26], La_2O_3/BiOCl[27], Y/BiOBr[28], and etc, the deep understanding of the influence of band and energy structure when rare earth doped is needed. The present investigations have mainly focused on the influence of rare earth doping on the light adsorption morphology control[29-30] separation efficiency of photo generated electron and holes.

In this paper, the effects of La doping on the band, energy structure and oxidation-reduction ability of BiOBr nano-sheets were evaluated in both theoretical and experimental research. Our research results confirmed that La doping could largely promote the oxidation ability of BiOBr, but inhibit its reduction.

1 Experimental

1.1 Reagents

All calcul ations were performed by using the first-principles density of functional theory (DFT), which were described by generalized gradient approximation (GGA) with the Perdew-Burke-Ernzerh of (PBE) exchange-correlation function. The calculations were applied the Cambridge Sequential Total Energy Package (CASTEP) calculation of materials studio software. During optimizations, the energy and force were converged to 10^{-5} eV·atom^{-1} and 0.25 eV·nm^{-1}, respectively. The plane-wave cut off energy was 340 eV. To simulate the La^{3+} doping, a 3×3×1 super cell was used. The *k*-points were 1×1×1 for optimizations.

1.2 Synthesis of La doped BiOBr (La-BiOBr) nanosheets

All chemicals were of analytical grade and used as received without further purification. The samples were obtained according to the previous report[31-32]. Under stirring, 0.01 mol cetyltrimethyl ammonium bromide (CTAB, as both surfactant and organic bromine source), NaBr (0.01 mol), and $Bi(NO_3)_3·5H_2O$ (0.02 mol) were added to ethylene glycol (EG, 40 mL), and obtained solution A. $La(NO_3)_3·6H_2O$ (0.16 mmol) and CTAB (0.48 mmol)was dissolved in 15 mL deionized water to obtain solution B. Then, solution B was slowly added into solution A under stirring. After further stirring for 1 h, the mixed solution was transferred into a Teflon-lined stainless steel autoclave and heated at 120 ℃ for 24 h. After cooling to room temperature, the samples were collected by centrifugation and washed with deionized water several times, then dried at 60 ℃ for 6 h.

1.3 Characterization

The samples were characterized by a series of physicochemical techniques. XRD patterns were obtained on an X-ray diffract meter (Panalytical Empyrean, Holland) at 40 kV and 40 mA for Cu $K\alpha$ (λ =0.154 06 nm). XRD test for samples scan range are as near as 2θ=10°~90°. The BET surface areas of the samples were obtained from N_2 adsorption/desor-

ption isotherms determined at liquid nitrogen temperature on an automatic analyzer (Micromeritics, ASAP 2020 HD88). The samples were degassed for 2 h under vacuum at 90 ℃ prior to adsorption measurements. SEM images were collected on a MLA650F scanning electron microscope operated at 20 kV, and were used to investigate the sample morphology. Transmission electron microscopy (TEM) images, high resolution TEM (HRTEM) and selected area electron diffraction (SAED) were recorded on a Tecnai G2-20 (FEI, USA, 200 kV). The absorption spectra of the sample were measured by UV-Vis spectrophotometer (UV-2550, Japan) with the $BaSO_4$ as the reference, and the scanning range was 200~700 nm. The room temperature photoluminescence (PL) emission spectra of the samples were recorded on a fluorescence spectrometer (Hitachi F-4500, Japan). The excitation light source was 350 nm. The chemical valences of elements and surface composition were analyzed by X-ray photoelectron spectroscopy (XPS, ESCALAB 250Xi). All the binding energies were referenced to the C1*s* peak at 284.8 eV of the surface adventitious carbon. Photocurrent and Mott-Schottky measurements were carried out on an electrochemical workstation with three-electrode (CHI 660E, China). 0.1 mol·L^{-1} Na_2SO_4 solution was used as electrolyte solution. Saturated Ag/AgCl and platinum wires were utilized as reference electrodes and the counter electrode, respectively.

1.4 Oxidative degradation of acid orange Ⅱ

The photo-catalytic oxidizability of the samples was determined by decomposition of acid orange Ⅱ in an aqueous solution under visible light irradiation (500 W Iodine-tungsten lamps). 0.05 g catalyst was dispersed in 100 mL of 0.02 g·L^{-1} acid orange Ⅱ. Before the lamp was turned on, the suspension was stirred in the dark for 30 min. During the reaction process, the suspension′s temperature was maintained at (20±2) ℃ by circulation of water. The aliquots of up to 3 mL were removed from the suspension, and the photo-catalyst particles in solution were removed by high speed centrifugation. The concentration of acid orange Ⅱ was determined by UV-Vis spectrophotometer.

1.5 Reduction of methylene blue

Herein, methylene blue dyes (MB) was as the reducing ability indicator by blue bottle experiment. The results of literature[33] shows that MB would be quickly reduced to leuco-methylene blue (LMB) under light irradiation by hole trapping of photo-catalyst, and the peak at 665 nm would be surely disappeared. Meanwhile, the photo-generated hole was certified as the oxidizing species of BiOBr. Therefore, ethylenediaminetetraacetic acid disodium salt (EDTA-2Na) was added into the methylene blue solution as the hole trapping of prepared photo-catalyst. The catalytic reduction process was the same as the degradation of acidic orange Ⅱ. The reduction rate was calculated by absorbance value at 665 nm of MB.

1.6 Degradation of ammonia nitrogen wastewater

0.05 g·L^{-1} ammonium chloride aqueous solution was used as simulated ammonia nitrogen wastewater. 0.05 g catalyst was dispersed in 100 mL 0.05 g·L^{-1} ammonium chloride solution. The catalytic degradation process was the same as the degradation of acidic orange Ⅱ. Nessler′s reagents spectrophotometer was used to measure the concentration of ammonia-nitrogen in aqueous solution[34]. In a typical measure, 1 mL ammonium chloride aqueous solution was mixed with added 50 mL deionized water in Nessler tube after being centrifuge. This was followed by 1 mL potassium sodium tartrate solution. After homogenizing, 1 mL Nessler reagent was added into the mixture solution. Its absorbance of 420 nm was measured by spectrophotometer.

The conversion ratio (R) of acid orange Ⅱ, methylene blue and ammonia nitrogen wastewater was determined by formula (**1**) as follow:

$$R=(1-C/C_0)\times 100\% \quad (1)$$

Where C_0 is the initial concentration of acid orange Ⅱ, methylene blue and ammonia nitrogen wastewater and C is the concentration after reaction.

2 Results and discussion

2.1 Crystallinity and texture analysis

The energy band structure is connected with the crystallinity and texture of photocatalyst. XRD pattern

was used to determine the crystalline phases and crystallinity of pure and La-BiOBr. In Fig.1(a), the sharp and intense diffraction peaks of samples indicated their high crystallinity. The XRD patterns of all samples exhibited the same diffraction peaks at 2θ of 10.9°, 25.2°, 31.7°, 32.3°, 46.3° and 57.2°. This crystal system was tetragonal and the space group was *P*4/*nmm*. The diffraction peaks are consistent with those of BiOBr (PDF No.01-085-0862), as indexed in Fig.1(a). The thicknesses of the vertical plane of different facets (*D*) were calculated by Braggs law. Then the cell parameters (nm) were also calculated by the relation between interplanar spacing and lattice parameter of tetragonal system, which was shown as formula (**2**).

$$\frac{1}{d^2}=\frac{h^2}{a^2}+\frac{k^2}{b^2}+\frac{l^2}{c^2} \quad (2)$$

Where d is the interplanar spacing, (hkl) is the Miller index, a, b and c are the lattice parameter. Table 1 shows the calculated results. It is clearly observed that the interplanar spacing of (001) and (110) facets were

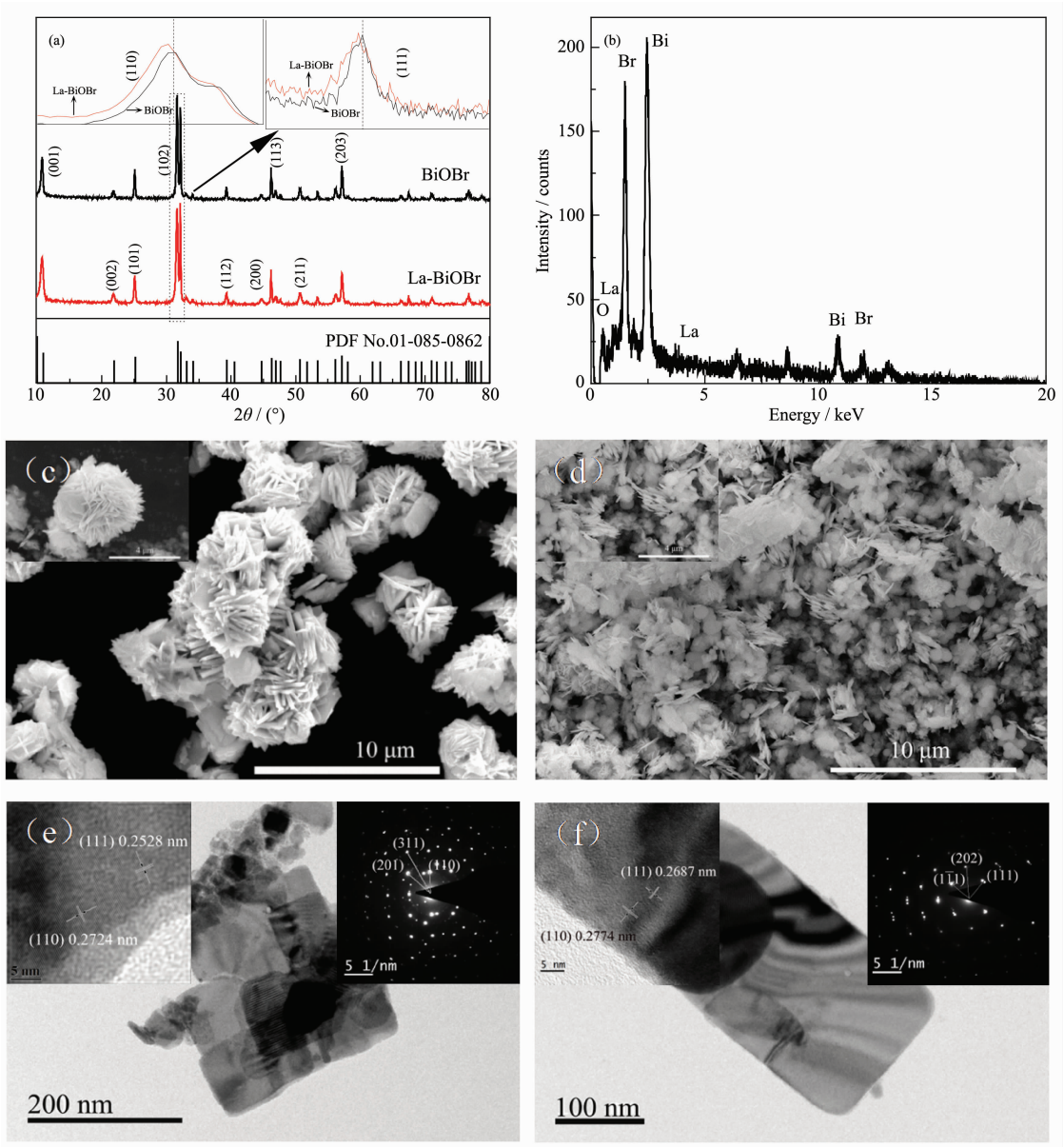

Fig.1 (a) XRD patterns of pure BiOBr and La-BiOBr samples, (b) EDX of La-BiOBr; SEM images of pure BiOBr (c) and La-BiOBr (d), the top left corner of (c, d) are magnified images of BiOBr and La-BiOBr; TEM images of pure BiOBr (e) and La-BiOBr (f), the top left corner of (e, f) are HRTEM of pure BiOBr and La-BiOBr respectively, and the top right corner of (e, f) are SAED of pure BiOBr and La-BiOBr respectively

Table 1　Thickness of the vertical plane of different facets of samples

Sample	*d* / nm		Cell parameter / nm		
	(001)	(110)	*a*	*b*	*c*
BiOBr	0.808 961	0.277 199	0.392 31	0.392 31	0.806 06
La-BiOBr	0.811 097	0.277 539	0.392 51	0.392 51	0.811 45

both increase with La doping. Meanwhile, the same variation also displayed in the cell parameters, which is consistent with the theoretical calculation. It means that lattice distortion may be induced by La doping.

EDX was used to verify whether La is present in the sample. As shown in Fig.1(b), the La element existed in the La-BiOBr sample. Fig.1(c,d) display the SEM images of BiOBr and La-BiOBr. Both of them are nano-sheets with thin thickness. But their aggregated state is slightly different. The micro topography of pure BiOBr is the nano-flower particles composed of nano-sheets. But the La-BiOBr nano-sheets assemble into thylakoid-like aggregation, indicating that the texture property may be changed by La doping. TEM, HRTEM and SAED further give us the results of the variations. As shown in Fig.1(e,f), the crystalline size of La-BiOBr became smaller than that of pure BiOBr, and its crystallization property was better. The crystalline interplanar spacing of BiOBr and La-BiOBr were 0.272 4 and 0.277 4 nm, respectively, showing the same results measured by XRD.

N_2 physical adsorption data are presented in Table 2. The BET surface area of BiOBr and La-BiOBr was 2 and 9 $m^2 \cdot g^{-1}$, respectively. Obviously, La-doping brings about two times increase in surface area. Moreover, the average crystalline size, pore volume and pore size are all influenced by La doping. With the La doped, the pore volume was increased. While the variation in pore diameter and crystalline size are on the contrary. The ionic radius of La^{3+} (117.2 pm) is larger than that of Bi^{3+} (110 pm). Therefore, La^{3+} doping induced the lattice distortion, which affects the crystalline size, and then brings about the variation in texture property.

Table 2　BET surface area (S_{BET}), pore size, pore volume, and average particle size of samples

Samples	S_{BET}[a] / ($m^2 \cdot g^{-1}$)	Pore volume[b] / ($cm^3 \cdot g^{-1}$)	Pore size[c] / nm	Average crystalline size[d] / nm
BiOBr	2	0.04	68.79	67.3
La-BiOBr	9	0.06	26.30	61.7

[a] BET surface area calculated from the linear part of the BET plot (p/p_0=0.05~0.3); [b] Total pore volume taken from the volume of N_2 adsorbed at p/p_0=0.995; [c] Average pore diameter estimated using the adsorption branch of the isotherm and the BJH formula; [d] Average crystalline size calculated from X-ray line broadening analysis of XRD results for the prepared pure BiOBr and La-BiOBr using Scherrer formula

2.2　Optical properties

Energy band structure of photo-catalyst is closely related to its optical properties. UV-Vis diffuse reflectance spectra (DRS) were applied to determine the light absorption ability of the fabricated samples. Fig.2(a) displays the UV-Vis DRS spectra of pure BiOBr and La-BiOBr samples. As shown in Fig.2(a), pure BiOBr has strong light absorption at 300~380 nm, and its absorption at visible spectrum (>420 nm) gradually decreases with the increase of light wavelength. With La doped, the fabricated La-BiOBr samples show obvious blue shift in absorption threshold. Tauc′s law was used to determine the band gap energies for the samples, which from the intercept of a straight line fitted through the rise of the function $(\alpha h\nu)^{1/2}$ plotted versus $h\nu$ and the results are shown in Fig.2 (b). Photoluminescence (PL) property of bare BiOBr and La doped BiOBr samples are shown in Fig.2(c). The excitation light source was 300 nm lasers. The PL emission peaks of all samples were near 460 nm, which was consistent with literature[35]. The PL intensity of the fabricated samples followed the order of BiOBr>La-BiOBr, which indicated that La doping could effective reduce the recombination of the

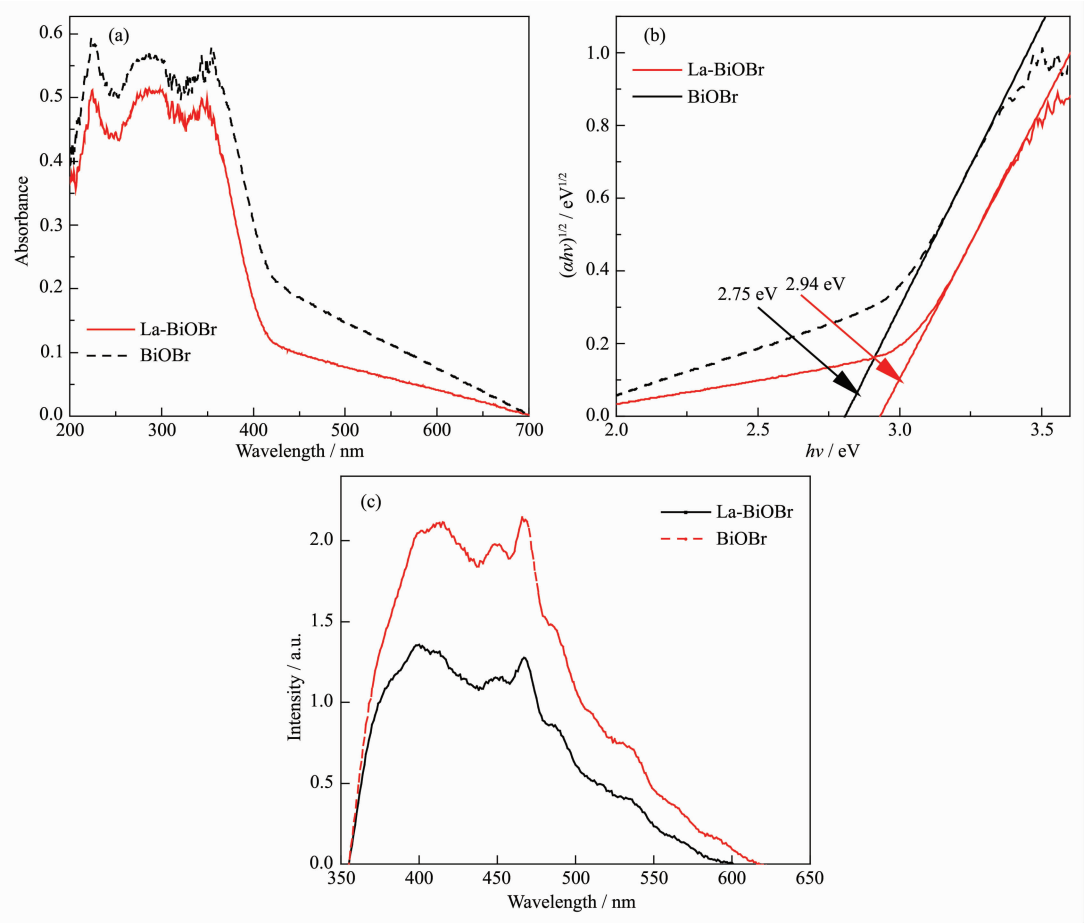

Fig.2 (a) UV-Vis spectra of the samples; (b) Plots of $(\alpha h\nu)^{1/2}$ versus energy ($h\nu$) for the band gap energy of samples; (c) PL spectra of the bare BiOBr and La doped BiOBr samples

photogenerated electrons and holes.

2.3 XPS analysis

XPS was used to investigate the valence state and the surface composition of elements in prepared samples. The typical XPS survey spectrum of La-BiOBr sample is presented in Fig.3(a), showing the existence of Bi, O, Br and La elements. Fig.3(b~e) shows high-resolution XPS spectra for four primary elements. As shown in Fig.3(b), the binding energy of 164.5 and 159.2 eV were for the Bi4$f_{5/2}$ and Bi4$f_{7/2}$ of Bi^{3+} in BiOBr, respectively[36]. Compared with BiOBr, there was a down shifted (~0.6 eV) of the Bi4*f* binding energy in La-BiOBr. The most likely cause of this condition was that La (1.10) have less electronegativity than Bi (2.02). Hence, the shell electron density of Bi would be increased with La doping, causing the value of Bi4*f* binding energy lower. This result is consistent with the theoretical calculation of DFT. The binding energies of La3$d_{5/2}$ at 837.5 eV and 3$d_{3/2}$ at 854.6 eV (Fig.3(c)) were indexed to La-O bond[37]. As for O1*s*, as shown in Fig.3(d), the peaks at 530.1 and 531.5 eV were ascribed to the oxygen attached to the which are lattice oxygen and the hydroxyl groups, respectively[38]. It was found that the binding energy of lattice oxygen in La-BiOBr was down shifted by 0.5 eV in comparison with that in pure BiOBr, which is believed to be related to La doping. Similarly, as shown in Fig. 3(e), the peaks of Br3$d_{5/2}$ and Br3$d_{3/2}$ in La-BiOBr were also down shifted by 0.5 eV compared with BiOBr. Based on XPS spectra together with XRD and TEM results, it is believed that La is doped in BiOBr.

2.4 Photo-catalytic activity of samples

The photo-catalytic performances of samples were evaluated by the degradation of acid orange Ⅱ (20 mg·L^{-1}), ammonia nitrogen waste water (50 mg·L^{-1}, pH=10), and the reduction of methylene blue (20 mg·

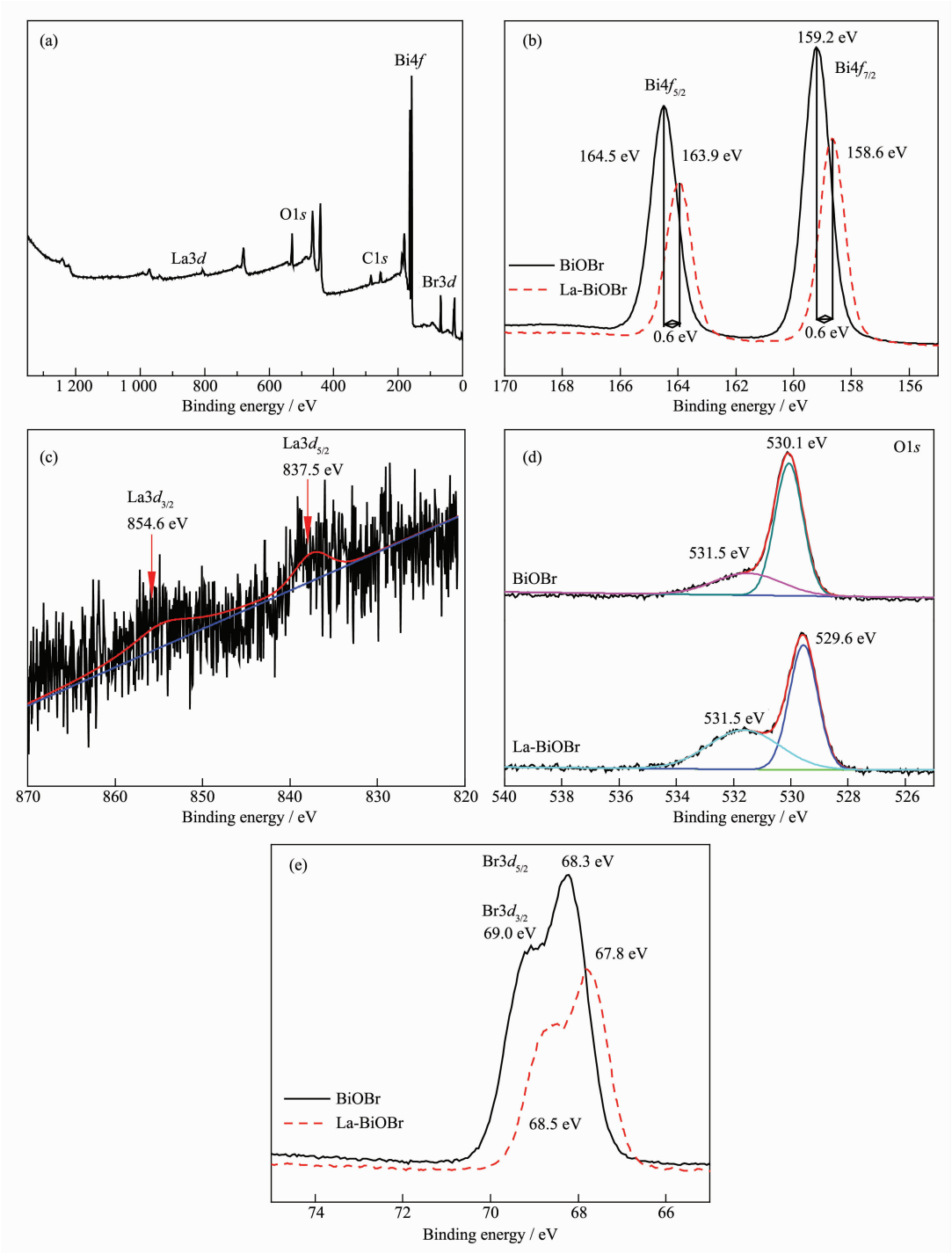

Fig.3　XPS spectra of La-BiOBr sample: (a) Survey spectrum; (b) Bi4*f*; (c) La3*d*; (d) O1*s*; (e) Br3*d*

L^{-1}). The conversion ratios (R) of acid orange Ⅱ, methylene blue and ammonia nitrogen wastewater were determined by formula (**1**). The results are shown in Fig.4. The degradation rates (conversion ratios) of acid orange Ⅱ over BiOBr and La-BiOBr were 74.1% and 90.5%, respe-ctively, indicating that the oxidation properties were significant improved by La doping. However, the reducing ability of BiOBr was decreased by La doping and the reduction rates for BiOBr and La-BiOBr were 64.84% and 50.7%, respectively. The degradation of ammonia nitrogen wastewater was tested to further verify the change of oxidation performance. In degradation of ammonia nitrogen, the reactions are shown as equations (**3**)~(**4**)[34]. The conversion rates of

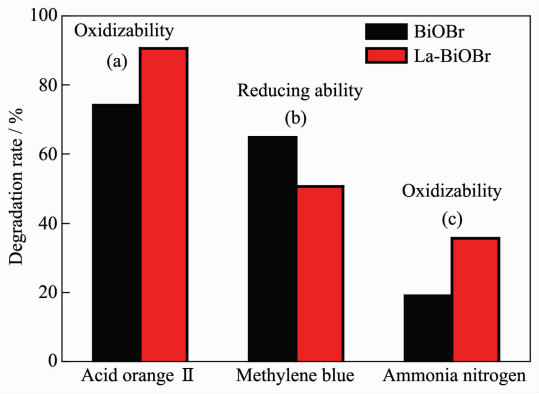

Fig.4 Photo-catalytic activity of samples: (a) Oxidizability for acid orange Ⅱ degradation; (b) Reducing ability for MB reduction; (c) Oxidizability for ammonia nitrogen wastewater degradation

ammonia nitrogen over BiOBr and La-BiOBr are 18.9% and 35.6%, respectively, which indicates that the oxidiza-bility of BiOBr was promoted by La doping.

$$NH_4^+ + 2OH^- \rightarrow NO_2^- + 3H_2 \quad (3)$$

$$2NO_2^- + O_2 \rightarrow 2NO_3^- \quad (4)$$

2.5 Discussion for the variation of oxidation-reduction ability

In order to illustrate the change of band positions of BiOBr induced by La^{3+} doping, the band positions of pure BiOBr and La-BiOBr were also calculated by the following formula[39]:

$$E_{VB} = X - E_e + 0.5E_g \quad (5)$$

$$E_{CB} = E_{VB} - E_g \quad (6)$$

where E_{VB} and E_{CB} are the valence band (VB) edge potential and the conduction band (CB) edge potential, respectively, X is the absolute electro-negativity of the semiconductor, E_e is the energy of free electrons on the hydrogen scale (the value of E_e is 4.5 eV), and E_g is the band gap energy of the semiconductor. Herein, the X value for BiOBr is 6.174 eV, the calculated result indicates that the CB and VB edge potentials of BiOBr were 0.3 and 3.05 eV, respectively. The value for La-BiOBr is 6.169 eV, so the CB and VB edge potentials of La-BiOBr are 0.2 and 3.14 eV, respectively. In addition, the Mott-Schottky curve obtained in an electrochemistry test (Fig.5(a)) was used to further confirm the changes of electronic structure of BiOBr induced by La doping. The results show that the BiOBr can be attributed to p-type semiconductor due to the negative slope of the linear plot. The flat band potentials of BiOBr and La-BiOBr electrodes are 0.024 and 0.01 V (vs Ag/AgCl, pH=7), respectively, which is equivalent to 0.224 and 0.21 V versus the normal hydrogen electrode (NHE, pH=7). Therefore, the calculated potentials of the top of VB for BiOBr and La-BiOBr are 2.974 and 3.15 V (vs NHE, pH =7), which is almost consistent with previous results of electronegativity calculation. These results indicated that the La doping could effectively improve the oxidation ability of holes in the VB of BiOBr.

The above analysis indicates that due to La doping, the VB of BiOBr was more positive and its CB

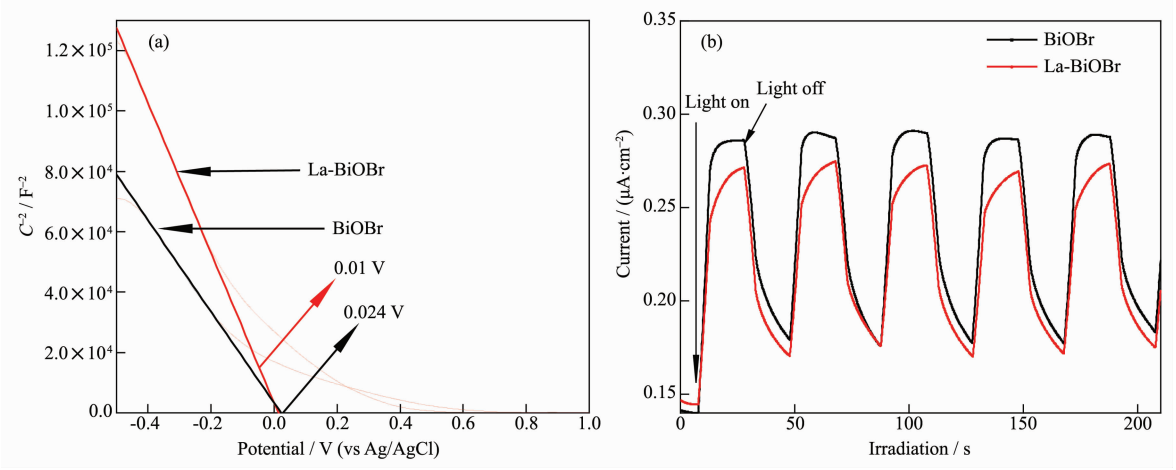

Fig.5 (a) Mott-Schottky (MS) plots for the pure BiOBr and La-BiOBr; (b) Photocurrent measurements of the pure BiOBr and La-BiOBr

was more negative. It seems that the oxidizability and reduction would be both improved by La doping. Hence, we think that a composite center of photo induced electrons may be formed by La doping, it made the electrons be trapped and inhibited the reduction of BiOBr. Due to the recombination centers for photo-generated charge carriers would cause significant photocurrent loss[40], photocurrent measurements were taken to verify the assumption. The results were shown in Fig.5(b). The photocurrent intensity of La-BiOBr was lower than BiOBr, indicating that La-BiOBr own less photo induced electrons which were consistent with our assumption.

2.6 DFT calculation

We constructed the model of La-doped BiOBr via the replacing Bi^{3+} by La^{3+} in BiOBr crystal, as shown in Fig.6(a). The substitution energy calculations indicated that the band gap of BiOBr was increased after La^{3+} doping (Fig.6(b)). Herein, the calculation result suggests that the band gap energies for BiOBr and La-BiOBr were 2.400 and 2.498 eV, respectively. It worth noticing that the variation of band band-gap energy induced by La doping have the property of larger band-gap energy (2.94 eV), which measured by UV-Vis DRS, is accordant with DFT calculation.

The calculated results show that the density of states (DOS) was also affected by La-doping. The DOS peaks of BiOBr at −20~−15 eV are mainly provided by the O2*s* atomic orbital, the DOS peaks of BiOBr at −15~−10 eV are mainly composed by the Br3*s* atomic orbital, and the DOS peaks of BiOBr at −10~−5 eV are mainly provided by the Bi6*s* atomic orbital. At the valence band area of BiOBr, the DOS of −5 to 0.3 eV are mainly provided by O2*p*, Br3*p* and trace Bi6*p*

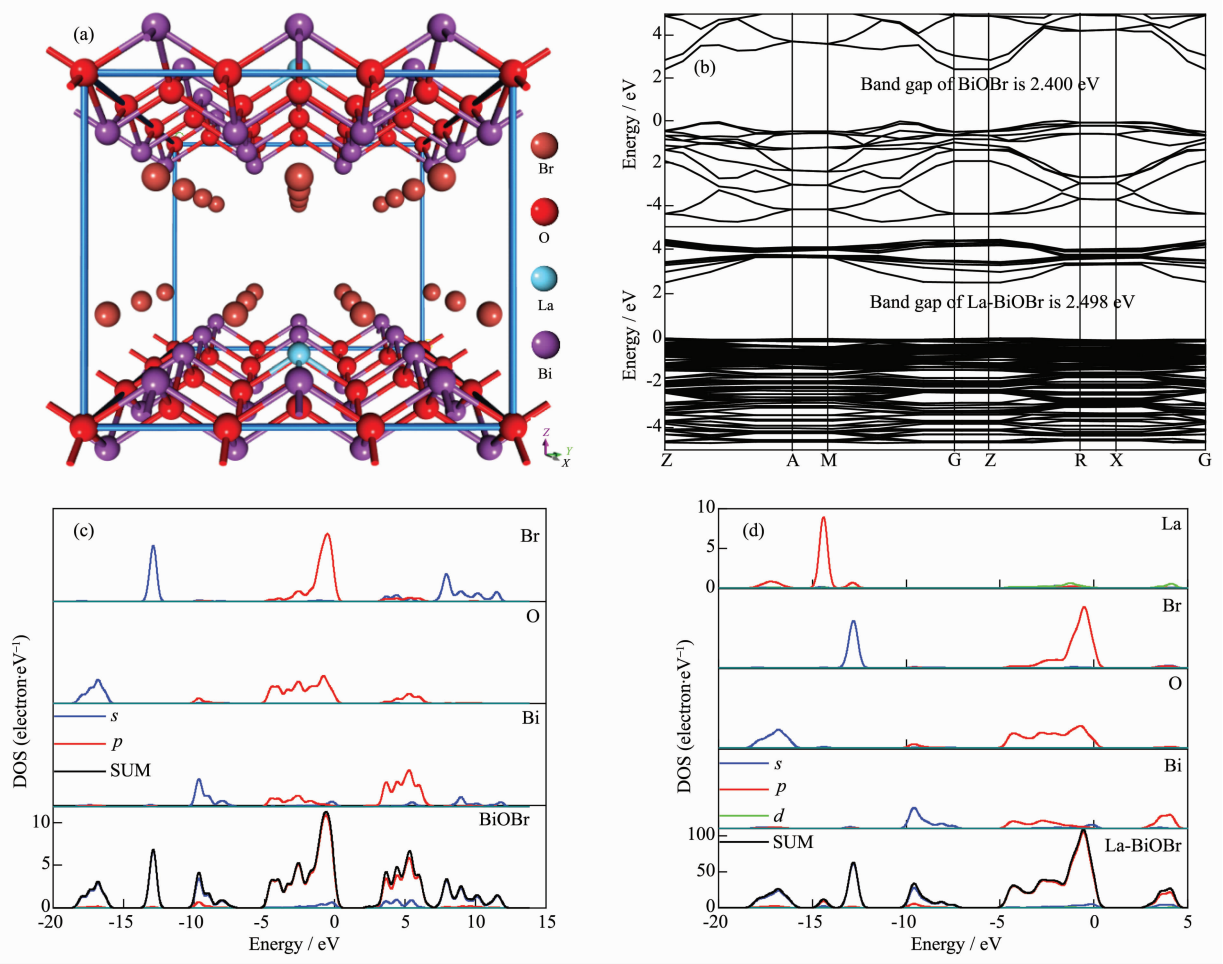

Fig.6 (a) La doped BiOBr model used in calculation, (b) band gap of bare and La doped BiOBr samples, the DOS of pure (c) and La doped (d) BiOBr samples

atomic orbital (Fig.6(c)). In La-doped BiOBr, the DOS peaks of BiOBr at −20 ~−15 eV arise from the contributions of La *p* and *d* orbital. A new DOS peak appears at −15~−14 eV which is attributed to the La *p* orbital. Meanwhile, the valence band at −5 ~0 eV and the conduction band at 0~5 eV are both provided by part of La *d* atomic orbital (Fig.6(d)). From Fig6(a), its worth noticing that the density of energy levels which with La doping was much higher than pure, manifested that the peak value of state density increased, and nearly 10 times (Fig6(c,d)). The similar variation also appeared in the article of Zhang et al.[41]. Zhang et al. think that rare earth ions were trivalent usually, two 6*s* electrons and 5*d* electrons in the outermost orbits would easily lose, then come into being free electrons or be captured by other ions. In this paper, it′s well known from Table 3 that atomic population of La is much smaller than Bi, indicating that it′s easier for La to lose electrons, the more electrons La lose, the more electrons system obtain, this is the reason why the peak value of state density increased nearly 10 times, consistent with the viewpoint of Zhang et al. as well. Meanwhile, we also notice that the localization of state density is increased with La doping, which lead to decrease the electro-conductivity of material, and likely increase the forbidden gap of semiconductor, thus have influence on the performance of photocatalysts. The corresponding results have been confirmed in the experiment. Hence, from the calculation results and electro negativity calculation, we much more confirmed that the doping of La^{3+} will change the oxidation and reduction ability of BiOBr because of the increase of band gap.

According to the above analysis, a possible photo catalytic reaction mechanism of La-BiOBr was proposed in Fig.7. Firstly, the above calculation has proved that La doping make the VB for BiOBr is more positive and the CB is slightly more negative, and La^{3+} formed an electron capture center of photo induced electrons. Hence more oxidizing species h^+ would be produced over La-BiOBr. On the contrary, its reduction performance was suppressed. Moreover, the results of XRD, N_2-physical adsorption and SEM indicated that the doping of La^{3+} could inhibit crystal growth and increase the surface area, which made the dyes adsorption easier. In consequence, the reaction tends to show the selective oxidation reaction and lower reducing property by La doping.

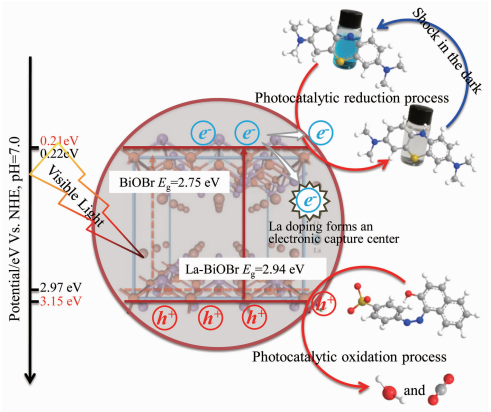

Fig.7 Schematic diagram of influence mechanism for oxidation-reduction ability of BiOBr by La doping

Table 3 Calculated bond population and bond length of pure BiOBr and La-BiOBr

Sample	BiOBr			La-BiOBr			
	Bi	O	Br	Bi	O	Br	La
Atomic populations	1.38	0.89	0.48	1.40	0.88	0.47	0.84
Bi-O bond populations	0.43				0.28		
La-O bond populations		—			0.31		
Bi-O bond length / nm		0.234 19			0.234 22		
La-O bond length / nm		—			0.245 11		

3 Conclusions

La-BiOBr with thylakoid structure photo-catalyst was obtained via solvothermal method. CTAB and NaBr were used as mixed bromine source. Doping of La^{3+} can inhibit growth of BiOBr crystals and promote

the stacking crystals, resulting in the unique thylakoid morphology. Moreover, La^{3+} doping resulted in the change in the energy band structure of BiOBr. With respect to pure BiOBr, a more positive potential of VB and a more negative CB were formed in La^{3+} doped BiOBr. At the same time, electron capture center was formed by La^{3+} doping, which make the performance of oxidation and reduction of BiOBr be promoted and inhibited, respectively.

Acknowledgments: This work was supported by National Natural Science Foundation of China (Grant No.21567008), Program of 5511 Talents in Scientific and Technological Innovation of Jiangxi Province (Grant No.20165BCB18014), Academic and Technical Leaders of the Main Disciplines in Jiangxi Province (Grant No.20172BCB22018), the Fund of Science and Technology in Jiangxi Province Department of Education (Grant No.GJJ150630), the Innovation Fund Designated for Graduate Students of Jiangxi Province (Grant No. YC2016-B076), the Innovation Project for Industrial Technological of Ganzhou (2015), the Outstanding Doctoral Dissertation Project Fund of JXUST (Grant No.YB2016006), the Researching Fund of JXUST (Grant No.NSFJ2015-G08), and Undergraduate Training Programs for Innovation and Entrepreneurship of JXUST (Grant No.DC2017-014).

References:

[1] FAN Qi-Zhe(樊启哲), ZHONG Li-Qin(钟立钦), FENG Lu-Ping(冯庐平), et al. *Materials Review*(材料导报), **2017**,**31**(9):106-111

[2] Tian J, Wu Z, Liu Z, et al. *Chin. J. Catal.*, **2017**,**38**:1899-1908

[3] Tian J, Liu R Y, Liu Z, et al. *Chin. J. Catal.*, **2017**,**38**:1999-2008

[4] Jiao H P, Yu X, Liu Z Q, et al. *RSC Adv.*, **2015**,**5**:16239-16249

[5] Tang J T, Liu Y H, Li H Z, et al. *Chem. Commun.*, **2013**,**49**:5498-5500

[6] Wang Z L, Hu T P, Dai K, et al. *Chin. J. Catal.*, **2017**,**38**:2021-2029

[7] Zheng L H, Yu X J, Long M C, et al. *Chin. J. Catal.*, **2017**,**38**:2076-2084

[8] Zhang J, Das A, Assary R S, et al. *Appl. Catal., B*, **2016**,**181**:874-887

[9] Niu K, Xu Y, Wang H C, et al. *Sci. Adv.*, **2017**,**3**:e1700921

[10]Wang J S, Qin C L, Wang H J, et al. *Appl. Catal., B*, **2018**,**221**:459-466

[11]Li X, Wen J Q, Low J X, et al. *Sci. China Mater.*, **2014**,**57**:70-100

[12]Wang X C, Maeda K, Thomas A, et al. *Nat. Mater.*, **2009**,**8**:76-80

[13]Ma S, Xu X M, Xie J, et al. *Chin. J. Catal.*, **2017**,**38**:1970-1980

[14]Chen F, Yang H, Luo W, et al. *Chin. J. Catal.*, **2017**,**38**:1990-1998

[15]Zhou X F, Li X, Gao Q Z, et al. *Catal. Sci. Technol.*, **2015**,**5**:2798-2806

[16]Li H, Shang J, Ai Z H, et al. *J. Am. Chem. Soc.*, **2015**,**137**:6393-6399

[17]PAN Jin-Bo(潘金波), LIU Jian-Jun(刘建军), MA He-Cheng(马贺成), et al. *Chinese J. Inorg. Chem.*(无机化学学报), **2018**,**34**(8):1421-1429

[18]BAO Yue(鲍玥), ZHOU Min-Yun(周旻昀), ZOU Jun-Hua(邹骏华), et al. *Environmental Science*(环境科学), **2017**,**38**(5):2182-2190

[19]WANG Dan-Jun(王丹军), SHEN Hui-Dong(申会东), Guo Li(郭莉), et al. *Acta Scientiae Circumstantiae*(环境科学学报), **2017**,**37**(05):1751-1762

[20]TANG Chang-Cun(唐长存), LI Yong-Gang(李永刚), HUANG Ying-Ping(黄应平), et al. *Journal of Molecular Catalysis (China)*(分子催化), **2017**,**31**(2):169-180

[21]WANG Yuan-You(王元有), GONG Ai-Qin(龚爱琴), YU Wen-Hua(余文华). *Chinese J. Inorg. Chem.*(无机化学学报), **2017**,**33**(3):509-518

[22]XUE Shuang-Shuang(薛霜霜), HE Hong-Bo(何洪波), WU Zhen(吴榛), et al. *Nonferrous Metals Science and Engineering*(有色金属科学与工程), **2017**,**8**(1):86-93

[23]LI Na(李娜), WANG Ming(王茗), ZHAO Bei-Ping(赵北平), et al. *Chinese J. Inorg. Chem.*(无机化学学报), **2016**,**32**(6):1033-1040

[24]Meksi M, Turki A, Kochkar H, et al. *Appl. Catal., B*, **2016**,**181**:651-660

[25]Yi J, Zhao Z Y. *J. Lumin.*, **2014**,**156**:205-211

[26]Dash A, Sarkar S, Adusumalli V N K B, et al. *Langmuir*, **2014**,**30**:1401-1409

[27]CHEN Jian-Chai(陈建钗), YU Chang-Lin(余长林), LI Jia-De(李家德), et al. *J. Inorg. Mater.*(无机材料学报), **2015**,**30**:943-949

[28]He M Q, Li W B, Xia J X, et al. *Appl. Surf. Sci.*, **2015**,**331**:170-178

[29]Ai Z H, Wang J L, Zhang L Z. *Chin. J. Catal.*, **2015**,**36**:2145-2154

[30]Huo Y N, Zhang J, Miao M, et al. *Appl. Catal., B*, **2012**,**111-112**:334-341

[31]LI Xin-Yu(李新玉), FANG Yan-Fen(方艳芬), XIONG Shi-Wei(熊世威), et al. *Journal of Molecular Catalysis*(*China*)(分子催化), **2013**,**27**(6):575-584

[32]FANG Jun-Hua(方俊华), ZHANG Kai(张凯), ZHANG Wei(张伟), et al. *Journal of the Chinese Ceramic Society*(硅酸盐学报), **2017**,**45**(4):572-578

[33]Mills A, Lawrie K, Mcfarlane M. *Photochem. Photobiol. Sci.*, **2009**,**8**:421-425

[34]Luo X P, Chen C F, Yang J, et al. *Int. J. Environ. Res. Public Health*, **2015**,**12**:14626-14639

[35]Zhou W, Hu X L, Zhao X R, et al. *J. Mol. Catal.*, **2014**,**28**:367-375

[36]Wang P Q, Yang P, Bai Y, et al. *J. Taiwan Inst. Chem. Eng.*, **2016**,**68**:295-300

[37]Gunasekaran N, Rajadurai S, Carberry J J, et al. *Solid State Ionics*, **1994**,**73**:289-295

[38]Liu Z S, Wu B T, Niu J N, et al. *Mater. Res. Bull.*, **2015**,**63**:187-193

[39]Yu C L, Wu Z, Liu R Y, et al. *Appl. Catal., B*, **2017**,**209**:1-11

[40]Bai S, Jin Y Z, Liang X Y, et al. *Adv. Energy Mater.*, **2015**,**5**:1401606

[41]ZHANG Li-Ying(张丽英), ZHANG Wei-Lei(张文蕾), MA Mei(马梅), et al. *Journal of Yili Normal University*: *Natural Science Edition*(伊犁师范学院学报:自然科学版), **2014**,**8**(1):38-42